Optimized design of self-powered SSHI interface circuit for enhanced vibration energy harvesting

Bin Zhang[a, b], Guang Yang[a], Bingxin Hu[a], Yeping Xiong[c], Shengxi Zhou[d,*]

[a] School of Mechanical, Electrical & Information Engineering, Shandong University, Weihai 264209, China

[b] Preparation and Application of Aerospace High-Performance Composite Materials, Future Industry Laboratory of Higher Education Institutions in Shandong Province, Shandong University, Weihai 264209, China

[c] Faculty of Engineering and Physical Sciences, University of Southampton, SO16 7QF, UK

[d] School of Aeronautics, Northwestern Polytechnical University, Xi'an 710072, China

Corresponding Author: Shengxi ZHOU: zhoushengxi@nwpu.edu.cn;

Abstract: Vibrational energy in ambient environment can be transformed into electrical power through piezoelectric energy harvesters and using synchronized switch harvesting on inductor (SSHI) techniques can significantly improve energy extraction efficiency. To enhance energy harvesting efficiency, this study proposes an efficient self-powered parallel SSHI (ESP-PSSHI) interface circuit. It enhances the passive peak detection switch, simplifies the circuit topology, reduces switching delay, and minimizes the "second inversion", contributing to increased energy harvesting efficiency. To improve the impedance-matching characteristics of the circuit, the proposed circuit is combined with a DC-DC converter module and finally, a stable electrical output is achieved. The performance of the ESP-PSSHI circuit in power generation is analyzed through simulation and subsequently verified via experimentation. Experiments show that the maximum output power of the ESP-PSSHI circuit is 2.42 and 1.16 times higher than the output power of the standard energy harvesting (SEH) circuit and self-powered parallel SSHI (SP-PSSHI) circuit, respectively. Through capacitor charging experiments, it is concluded that the output power of the optimized ESP-PSSHI circuit is 1.5 times the output power of the LTC3588-1 circuit.

Keywords: piezoelectric; energy harvesting; interface circuit; efficient self-powered parallel SSHI

1 Introduction

Low-powered microelectronic devices have become increasingly common in environmental monitoring, structural health monitoring, industrial manufacturing, and other fields as science and technology advances[1-3]. Wireless sensor networks (WSNs) have been limited in their development by the inability to provide long-term stable

power. Most of these electronic devices depend on chemical batteries for power supply. However, chemical batteries pose several problems, such as large size and short life span, as well as environmental pollution. Therefore, a number of researchers have focused their attention on environmental energy harvesting techniques. Various forms of energy are available in the environment for our utilization, such as solar energy, wind energy, thermal energy, and vibration energy. In certain applications, due to limitations such as climate conditions, vibration energy may be the sole source of energy. Piezoelectric vibration energy harvesting possesses advantages over electrostatic and electromagnetic methods in terms of ease of miniaturization and high energy density[4, 5]. For this reason, using the piezoelectric energy harvester (PEH) to convert environmental vibration energy into electrical energy for long-term and efficient energy supply of electronic products has become a hot research topic[6-9]. On this basis, the paper will design the interface circuit for piezoelectric energy harvesting to increase the output power of PEH and manage the output electrical energy to realize the effective utilization of environmental vibration energy.

Output electrical energy of PEHs is in alternating current (AC), while most current wireless sensor devices require direct current (DC) power [10-13]. As a result, it is essential to design an interface circuit that can convert the AC power output from the PEH to DC power [14, 15]. Four classic circuits can convert AC to DC, among which the SEH circuit is the easiest to implement, consisting of four diodes and a filter capacitor [16]. It has the advantage of being simple, stable, and reliable. However, the voltage and current output of the SEH circuit exhibit an excessive phase discrepancy, which reduces the energy extraction efficiency, and the load has an impact on the output power. To improve energy harvesting efficiency, Guyomar *et al*. [17] introduced the parallel SSHI (P-SSHI) circuit as an extension to the SEH circuit. The P-SSHI circuit is designed to rapidly reverse the voltage across a piezoelectric material (PZT) through control of both the switch and inductor. This modification reduces the reactive power and increases the efficiency of energy harvesting. Taylor *et al*. [18] presented a series SSHI (S-SSHI) circuit, which connected the PZT in series with the electronic switch and inductor, using the switch on and off to nonlinearly synchronize the voltage generated by the PZT, improving the output efficiency. However, the control of its switching time is more complicated. To make that the circuit output power is independent of the load, Lefeuvre *et al*. [19] designed the synchronous electric charge extraction (SECE) circuit, which was decoupled through the implementation of Buck-Boost converters. The SECE circuit has been widely studied by researchers due to its insensitivity to loads effects on its output power. Wu *et al*. [20] proposed an optimized SECE technique, which improves the conversion efficiency and broadband characteristics compared to the SECE. Brenes *et al*. [21] proposed the frequency-tuning

SECE technique, which potentially doubles the bandwidth energy harvesting capacity compared to the latest bandwidth enhancement techniques. The SECE circuit exhibits stable output performance, however, the energy harvesting efficiency is impacted by the control accuracy of the electronic switch. The SSHI technology, on the other hand, has a much more stable operating performance than the SECE technology, even though its output power depends on the load. Chen *et al*. [22] proposed a self-powered multi-input SSHI circuit capable of harvesting energy from via piezoelectric ceramics with different phases. Wang *et al*. [23] designed a rectifier-less synchronized switch harvesting on inductor interface circuit, which operates in the S-SSHI circuit mode during the positive half-cycle and in the P-SSHI circuit mode during the negative half-cycle. Experimental results showed that the maximum output power of the circuit is significantly higher than the maximum output power of the S-SSHI circuit. In general, the P-SSHI circuit not only has better broadband characteristics than the S-SSHI circuit, but can also harvest more energy. It is currently considered to be an efficient interface circuit for energy harvesting [24]. It should be noted that the power comparison of the above interface circuits is based on the fact that PEH works under weak electromechanical coupling conditions. Under medium electromechanical coupling or strong electromechanical coupling conditions, the influence of electromechanical coupling coefficient on the whole system needs to be further considered [25].

Several improvements have been made to the P-SSHI circuit in order to maximize the energy harvesting efficiency. Lu *et al.* [26] proposed a rectifier circuit based on the P-SSHI technique, which uses two comparators to monitor the voltage of a piezoelectric element and uses a pulse signal to close an electronic switch to reverse the voltage. By combining the benefits of the SECE circuit and the P-SSHI circuit, Lallart *et al*. [27] designed a synchronous inversion and charge extraction (SICE) circuit. The output power of this circuit is five times as that of the SEH circuit. To extract more energy, Liang *et al*. [28] designed a parallel synchronized triple bias-flip (P-S3BF) circuit. The efficient extraction of energy was achieved by reasonably distributing the voltage inversion action. Experimental results showed that the output power of this circuit was increased by 24.5% relative to that of the P-SSHI circuit. Du *et al*. [29] proposed an SSHI circuit with a cold start function, which enabled the PEH to start from a cold state with even a low-level excitation. The purpose of this scheme is to promote the development of a self-powered interface circuit. Badr *et al*. [30] proposed the NVC-PSSHI circuit by using a trigger circuit and a negative voltage converter (NVC) for the P-SSHI circuit, which implemented both cold start and self-powered functions. However, all the above circuits require an external power supply or other auxiliary circuit system for peak detection and switching control while improving energy harvesting efficiency. This not only increases the complexity of the circuits, but also

does not meet the current demand for self-powered nodes in wireless sensing networks. To simplify the circuit and realize the self-powered function, Lallart *et al*. [31] designed a passive peak detection circuit and used this electronic switch to design a self-powered P-SSHI circuit. Liang *et al*. [32] designed a self-powered SSHI circuit. To reduce the negative effect of "second inversion" caused by the transistor parasitic capacitance in passive peak detection circuits, Liu et al. [33] designed an optimized self-powered P-SSHI circuit, but the circuit has a large switching delay. However, the passive peak detection circuit utilized in the above interface circuit used too many electronic components, which raised the internal losses and decreases its efficiency. Therefore, in this paper, the passive peak detection switch will be improved to increase the power output.

Although the P-SSHI circuit has high energy harvesting efficiency and broadband characteristics, its output power varies considerably under different loads, which hinders its further use in wireless sensing. In recent years, researchers have investigated impedance matching techniques that can significantly improve energy harvesting efficiency when the internal impedance of the PZT is matched to the impedance of the circuits [34-36]. In order to achieve impedance matching, Li *et al*. [37] proposed a perturbation observation algorithm for tracking the maximum power of P-SSHI circuits and experimentally showed that the technique could achieve a maximum tracking efficiency of up to 97%. Chew *et al*. [38] designed a high-pass filter circuit which is capable of tracking half of the PZT open circuit voltage to achieve maximum power output. However, the use of the above technique for maximum power monitoring requires the PZT to be disconnected from the load and therefore results in a loss of energy. To reduce energy losses, Sharma *et al*. [39] designed a damped tuned circuit. It obtained the maximum power point by monitoring the frequency information of the PEH. When the operating state of the PEH changed, the circuit was able to automatically adjust the electrical damping without disconnecting from the load. Thus, the electrical damping matched with the mechanical damping, resulting in a higher energy output. In the above mentioned interface circuits, a large number of external control circuits are used in order to achieve impedance matching, which increases the internal losses and instability of the circuit and makes it difficult for the circuit to be self-powered.

To overcome the various problems in the above interface circuits, an efficient SP-PSSHI circuit based on the P-SSHI circuit is proposed in this paper. The use of diodes and resistors in the passive detection switch is reduced, while two inductors are set up, and the positive/negative peak detection circuits operate with different inductors, effectively reducing the effects of “second inversion”. In this way, the switching delay of the circuit is reduced while the internal losses are decreased. Thus, the effectiveness

of energy harvesting is increased. In order to improve the impedance matching characteristics of the circuit, this paper continues to optimize the proposed circuit. By using a DC-DC converter and a properly designed external circuit, the PEH outputs the stable power supply. The superiority of the designed circuit is demonstrated in simulations and experiments.

2 Analysis of the PZT equivalent circuit model and interface circuits

2.1 Equivalent circuit model of the PZT

When an external force deforms a PZT, its internal polarization occurs, generating positive and negative charges on its two opposite surfaces, thus forming an electric current. Figure 1 depicts an electromechanical coupling model of the PZT. L_m is the mechanical mass; C_k is the mechanical strength; R_b is the mechanical damping; n is the coupling coefficient; and C_P is the internal capacitance of the PZT. Since this study is based on the cantilever piezoelectric vibration energy harvester, its electromechanical coupling coefficient is very low. Therefore, the establishment of the equivalent circuit model and the formula derivation of the interface circuit power in this paper are based on the PEH working under the condition of weak electromechanical coupling [40]. When the PEH operates under resonant conditions, the electromechanical coupling model can be simplified to the corresponding uncoupled model as illustrated in Figure 2. Where the current source I_P, capacitor C_P, and resistor R_P are connected in parallel to form an equivalent circuit model[41].

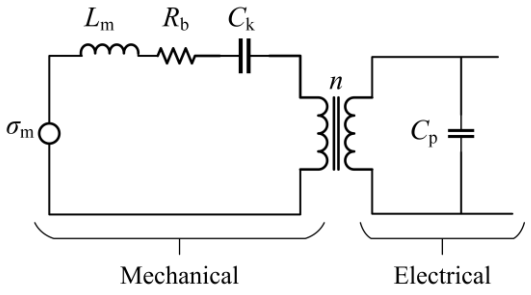

Figure 1 Electromechanical coupling model

2.2 Analysis of SEH

The early interface circuit utilized in PZT energy harvesting, the SEH circuit, is depicted in Figure 2. Four diodes and a filter capacitor make up its fundamental structure. When the PEH is subjected to sinusoidal excitation, its vibration displacement

and output voltage are shown in Figure 3. When the beam moves in the positive direction, the voltage of the PZT increases continuously. When the voltage of the PZT is greater than the load voltage, the rectifier bridge is turned on, and the current begins to flow to the load. Due to the clamping effect of the filter capacitor, the voltage of the PZT remains unchanged. When the PZT moves to the maximum positive displacement and begins to move in the opposite direction, the current direction changes from positive to negative, and the PZT is reversely charged. The working process of the circuit in the negative half cycle is similar to that in the positive half cycle. However, due to the internal parasitic capacitance of the PZT, this circuit has excessive reactive power during rectification, which reduces the energy harvesting efficiency [42].

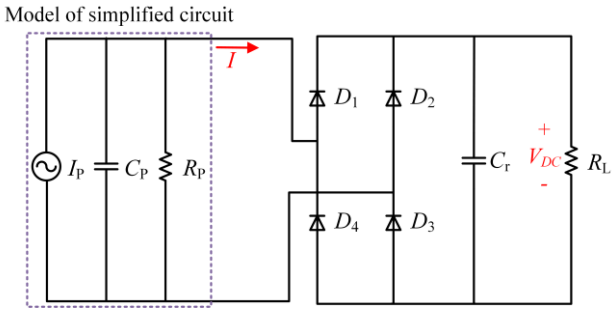

Figure 2 Schematic of the SEH circuit

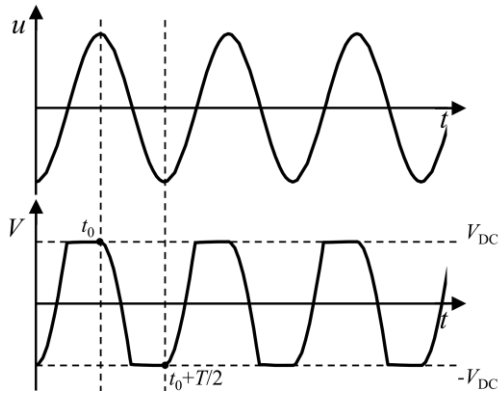

Figure 3 Theoretical waveform of SEH circuit

When the electromechanical coupling of the PEH is weak, the energy harvested by the PEH is negligible compared to the external input. Hence, the excitation displacement U_M of the PEH remains essentially constant. The voltage across the load can be shown as the following equation when the voltage drop V_d of the diode is neglected[43]:

$$V_{DC} = \frac{2\alpha U_M \omega R_L}{2R_L C_P \omega + \pi} \tag{1}$$

The corresponding output power is stated as:

$$P = \frac{V_{DC}^2}{R_L} = \frac{4\alpha^2 U_M^2 \omega^2 R_L}{(2R_L C_P \omega + \pi)^2} \tag{2}$$

Analysis of the aforementioned equation demonstrates that the output power varies with the load, making $dP/dR_L=0$, the optimal load can be obtained as:

$$R_{opt} = \frac{1}{4fC_P} \tag{3}$$

The corresponding maximum output power at this point can be expressed as [44]:

$$P_{max} = \frac{\omega\alpha^2 U_M^2}{2\pi C_P} \tag{4}$$

where ω is the circular frequency of excitation and α is the force factor.

2.3 Analysis of P-SSHI

Despite its simple structure, the SEH circuit generates excessive reactive power during operation, resulting in wasted energy. To solve this problem, researchers have improved the SEH circuit by rationalizing the design of the circuit structure and using the synergy of the electronic switch and the inductor, reducing energy losses. The topology of the circuit is shown in Figure 4. An external auxiliary circuit is required to control the switch in this circuit. When the PEH is subjected to sinusoidal excitation, its vibration displacement and output voltage are shown in Figure 5. It can be seen from the waveform in the figure that when the PZT moves to the positive extreme value, the switch S is closed, and the internal capacitance C_P of the PZT and the inductance in the interface circuit constitute the LC oscillation circuit. After half the LC oscillation cycle, the switch S is disconnected. At this time, the voltage on the PZT reverses from the previous V_{DC} to $-V_m$.

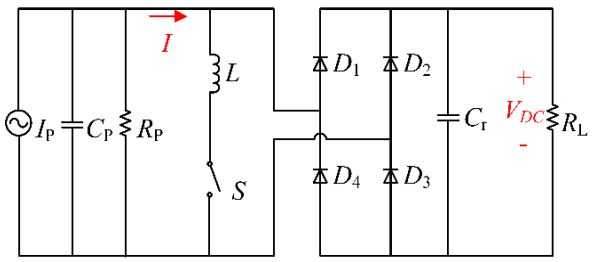

Figure 4 Schematic of the P-SSHI circuit

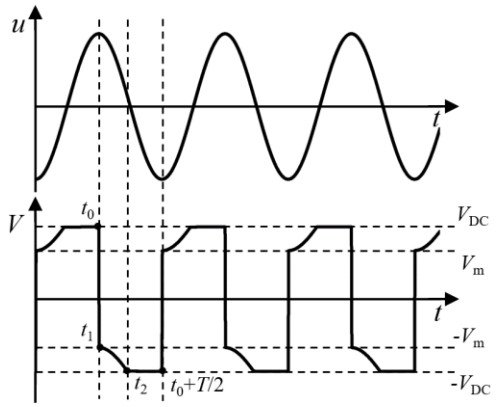

Figure 5 Theoretical waveform of P-SSHI circuit

Due to the presence of energy losses, there exists a ratio relationship γ between V_{DC} and V_m, which is defined as the inversion factor, and the expression is shown as:

$$\gamma = \frac{V_m}{V_{DC}}, (0 < \gamma < 1) \tag{5}$$

After the voltage reversal is completed, with the negative movement of the PZT, the voltage of the PZT continues to increase negatively. When the voltage rises to $-V_{DC}$, the rectifier bridge is turned on, and the PZT supplies power to the filter capacitor C_r and the load R_L. When the PZT moves to the negative extreme value, the rectifier bridge is disconnected, and the PZT no longer supplies power to the filter capacitor and the load. At this time, the switch S is closed again and the above process is repeated. The voltage V_{DC} across the load can be represented as following equation when the voltage drop V_d of the diode is disregarded[43]:

$$V_{DC} = \frac{2\alpha U_M R_L \omega}{(1-\gamma) C_P R_L \omega + \pi} \tag{6}$$

The output power may be calculated by using the given equation:

$$P = \frac{V_{DC}}{R_L} = \frac{4\alpha^2 U_M^2 \omega^2 R_L}{[(1-\gamma) C_P R_L \omega + \pi]^2} \tag{7}$$

From the above equation, it can be concluded that there is an optimal load for the circuit to maximize the output power. Let $dP/dR_L=0$ to obtain the optimal load, as follows:

$$R_{opt} = \frac{1}{2 f C_P (1-\gamma)} \tag{8}$$

According to the above equation, the output power can be derived as:

$$P_{\max} = \frac{\omega\alpha^2 U_{\mathrm{M}}^2}{\pi C_{\mathrm{P}}(1-\gamma)} \tag{9}$$

The above derivation reveals that the output power of the P-SSHI circuit is significantly higher than that of the SEH interface circuit.

3 Circuit design

As part of the design process for the efficient SP-PSSHI circuit, we have improved the peak detection circuit. Two inductors and four diodes are provided in the peak detection switch. The positive and negative peak detection switches operate with different inductors to reduce the effect of "second inversion" and to ensure the uniformity of energy flow. In order to reduce the forward voltage drop of the diodes, Schottky diodes are used in the circuit. The improved circuit ESP-PSSHI for the SP-PSSHI circuit is displayed in Figure 6, and Table 1 shows the models of the critical components in the illustration.

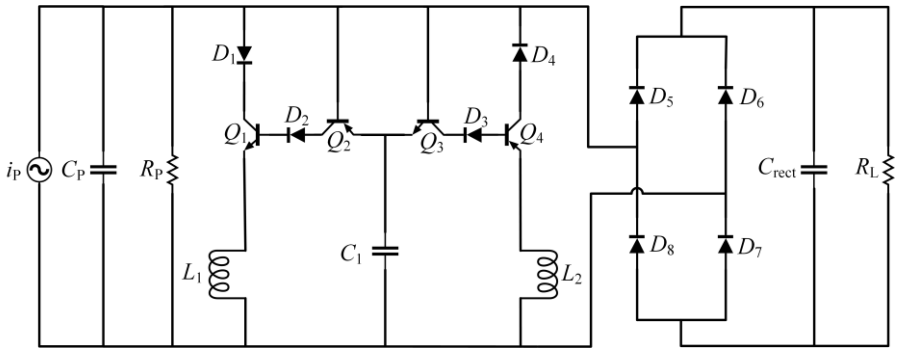

Figure 6 Schematic of ESP-PSSHI circuit

Table 1 Models of circuit components

Component	Model
D_1-D_8	SS34
Q_2, Q_4	TIP32C
Q_1, Q_3	TIP31C

In Figure 6, the principle of maximum value detection is similar to minimum value detection. Therefore, we will focus on the maximum value detection principle and analyze the operating characteristics of the ESP-PSSHI circuit in conjunction with the four stages of circuit operation. In the analysis process, combined with the theoretical waveform of the ESP-PSSHI circuit. When the sinusoidal excitation is applied to the

PZT, the corresponding AC voltage is generated, that is, the open circuit voltage V_{OC}. When the ESP-PSSHI circuit is connected, the voltage and current waveforms are shown in Figure 11. The four operating stages of the circuit works as follows:

Natural Charging: As the PZT moves from the initial position to the maximum displacement, the equivalent current source i_P begins to charge the circuit positively, and the PZT voltage and the peak detection capacitor voltage gradually increase, as shown in Figure 7. This process corresponds to the phase c to phase d in Figure 11. During the charging process, the rectifier bridge is disconnected at this stage because the voltage of the PZT is less than the on-state voltage of the rectifier bridge. The equivalent current source i_P and the internal capacitance C_P of the PZT, the peak detection capacitor C_1, form a charging circuit, and the current transfer path is $i_{P+} \rightarrow C_P // R_P \rightarrow i_{P-}$, $i_{P+} \rightarrow Q_3 \rightarrow C_1 \rightarrow i_{p-}$.

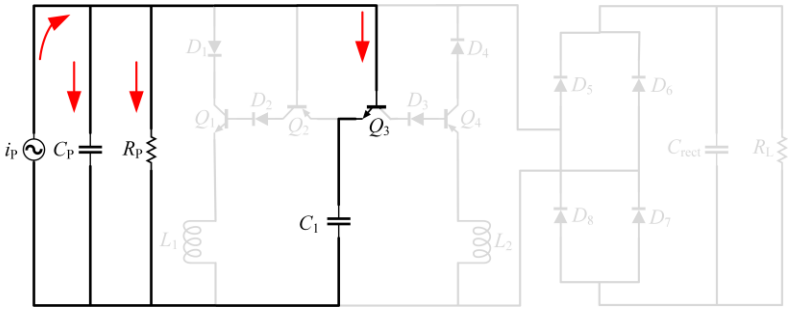

Figure 7 Natural charging stage of the ESP-PSSHI circuit

Energy extraction: Once the voltage of the PZT increases to the conduction voltage of the rectifier bridge, as depicted in Figure 8, the current passes through the filter capacitor C_{rect} and the load R_L, and energy extraction starts. During the conduction of the circuit, the voltage between the capacitors C_P and C_1 remains constant due to the clamping effect of the filter capacitor. This process corresponds to the phase d to phase e in Figure 11. In the energy extraction stage, the voltage of the PZT reaches the maximum V_M. At this time, the current transfer path is $i_{P+} \rightarrow C_P // R_P \rightarrow i_{P-}$, $i_{P+} \rightarrow D_5 \rightarrow C_{rect} // R_L \rightarrow D_7 \rightarrow i_{p-}$.

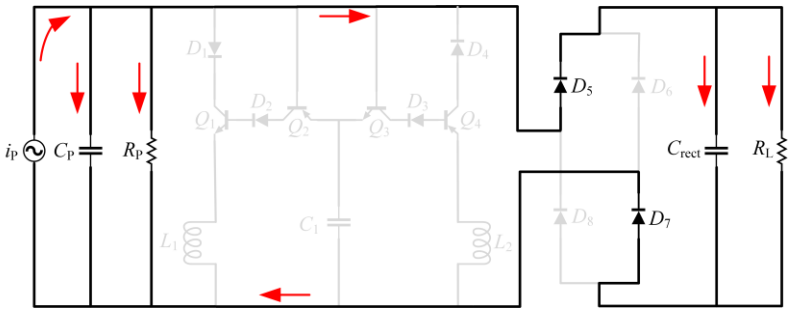

Figure 8 Energy extraction stage of the ESP-PSSHI circuit

Extra open circuit: When the PZT moves to the positive extreme, its output current is zero, and then it starts to move in the negative direction. The current source i_P charges the circuit in reverse, and the voltage across the PZT begins to decrease, and at this time, as shown in Figure 9, the rectifier bridge is disconnected. The voltage across the capacitor C_1 remains constant due to the threshold voltage of the transistor Q_2 and the reverse cutoff of the diode D_1. This process corresponds to the phase e to phase f in Figure 11. At this time, the current transfer path is $i_{p-} \rightarrow C_P // R_P \rightarrow i_{p+}$.

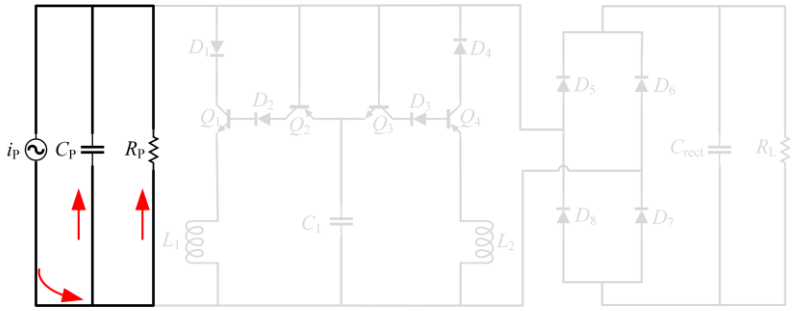

Figure 9 Extra open circuit stage of the ESP-PSSHI circuit

Voltage inversion: When the voltage difference between the PZT voltage and the peak detection capacitor C_1 is the threshold voltage V_{be} of the transistor, the transistor Q_2 conducts, while the transistor Q_1 is prompted to conduct, and then enters the voltage inversion stage, as seen in Figure 10. An LC resonant circuit is now formed by the inductor L_1 and the internal capacitor C_P of the PZT, with the current transfer path being $C_P \rightarrow D_1 \rightarrow Q_1 \rightarrow L_1 \rightarrow C_P$; At this time, the electrical energy within the peak detection capacitor is now beginning to be harvested, and the current transfer path is $C_1 \rightarrow Q_2 \rightarrow Q_1 \rightarrow L_1 \rightarrow C_1$. After a 1/2 resonant cycle, the PZT voltage reverses from the maximum value V_M to $-V_m$, this process corresponds to the phase f to phase g in Figure 11, the negative detection circuit begins to operate, and the circuit enters the negative half-cycle operation process.

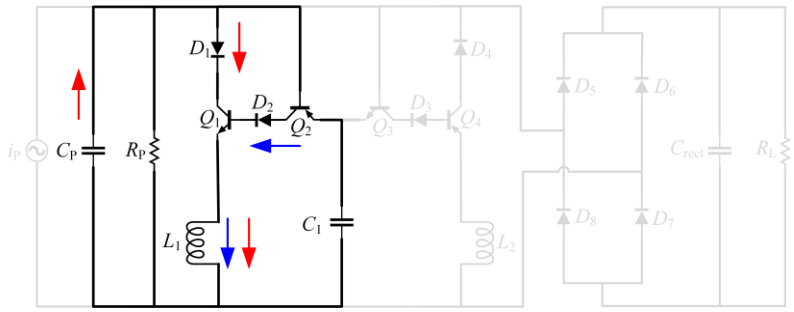

Figure 10 Voltage inversion stage of the ESP-PSSHI circuit

Figure 11 demonstrates that when the vibration displacement reaches an extreme value. Its voltage is not immediately reversed, which is caused by a switching delay in

the circuit. The switching delay causes energy dissipation, for which the energy loss can be reduced by optimizing the circuit structure.

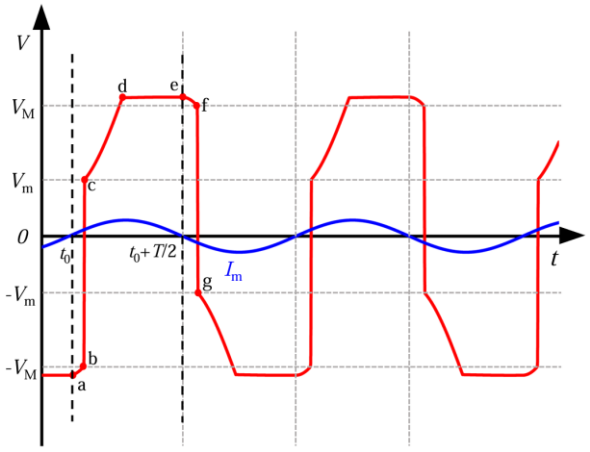

Figure 11 Output voltage waveform of ESP-PSSHI circuit

When the PZT is subjected to a harmonic excitation and its frequency is near the first-order resonant frequency of the PEH the equivalent current source can be expressed as:

$$I_m = I_M \sin(\omega t) \tag{10}$$

where I_M and ω are the current source amplitude and frequency, respectively. Combining equivalent electrical model of the PZT with Kirchhoff's current theorem, we can obtain the equivalent current I flowing out of the PZT, as follows:

$$I = I_M \sin(\omega t) - C_p \dot{V} \tag{11}$$

where C_P and V are the internal capacitance and voltage of the PZT, respectively. Assuming that the expression of the mechanical vibration displacement is:

$$u = -U_M \cos(\omega t) \tag{12}$$

The following equation can found:

$$I = \omega \alpha U_M \sin(\omega t) - C_p \dot{V} \tag{13}$$

Combining equations (11) and (13) yields:

$$I_M = 2\pi f \alpha U_M \tag{14}$$

where U_M and α are the vibration amplitude and the force factor, respectively.

The following formula illustrates the connection between the open-circuit voltage

and the current source current:

$$V_{\mathrm{OC}} = \frac{I_{\mathrm{M}}}{\omega C_{\mathrm{P}}} = \frac{\alpha U_{\mathrm{M}}}{C_{\mathrm{P}}} \tag{15}$$

During half an operating cycle, i.e., the time period from point a to point e in Figure 11. The PZT voltage varies during a half-cycle when it is not linked to the interface circuit as:

$$\Delta V = 2V_{\mathrm{OC}} \tag{16}$$

When the ESP-PSSHI circuit is connected, the analysis starts from a in Figure 11. When the PZT moves to the extreme value of the negative direction and will move in the inverse direction, the voltage across the PZT at this moment $-V_{\mathrm{a}}$ is:

$$-V_{\mathrm{a}} = -(V_{\mathrm{DC}} + 2V_{\mathrm{D}}) \tag{17}$$

where V_{DC} denotes the voltage across the load resistor. The capacitor C_1 voltage V_{C1} at the moment of point a is:

$$V_{\mathrm{C1}} = -(V_{\mathrm{a}} - V_{\mathrm{be}}) \tag{18}$$

where V_{be} is the transistor base emitter conduction voltage value. The voltage of the PZT starts decreasing with the inverse vibration, while the voltage across capacitor C_1 stays as a constant. When the difference between the voltage of the PZT and the voltage of C_1 is V_{be}, Q_3 conducts, i.e., at moment b. At this time, the value of the voltage across the PZT $-V_{\mathrm{M}}$ can be expressed as:

$$-V_{\mathrm{M}} = V_{\mathrm{c1}} + V_{\mathrm{be}} \tag{19}$$

Q_3 conducts and then prompts Q_4 to conduct, at which time the voltage of the PZT begins to invert, from $-V_{\mathrm{M}}$ at moment b to V_{m} at moment c. Due to energy loss, the voltages before and after the inversion are shown below.

$$V_{\mathrm{m}} = \gamma V_{\mathrm{M}} = e^{-\frac{\pi}{2Q}} V_{\mathrm{M}} \tag{20}$$

where γ is the inversion factor ($0<\gamma<1$) and Q represents the quality factor of the LC resonant circuit. The equation shown below can be used to describe Q.

$$Q = \frac{1}{R}\sqrt{\frac{L}{C}} \tag{21}$$

By analyzing equations (20) and (21), we can observe that the inversion factor γ has a direct correlation with the quality factor Q of the LC resonant circuit. Therefore, the quality factor of the circuit can be enhanced by choosing suitable electronic components to improve energy harvesting efficiency.

When no energy extraction is carried out, analysis of equations (10) to (20) reveals that the amount of voltage change of the PZT after connecting the interface circuit for half a vibration cycle (time period of Fig. 10a~e) can be stated as:

$$V_{\mathrm{e}} = -V_{\mathrm{a}} + \Delta V + V_{\mathrm{M}} + V_{\mathrm{m}} \tag{22}$$

Then the energy transformed by the circuit during half a vibration cycle can be derived as:

$$W = V_{\mathrm{DC}} C_{\mathrm{P}} (V_{\mathrm{e}} - V_{\mathrm{a}}) = V_{\mathrm{DC}} C_{\mathrm{P}} [2V_{\mathrm{OC}} + (\gamma - 1)V_{\mathrm{DC}} + (2\gamma - 2)V_{\mathrm{D}} - (2\gamma + 2)V_{\mathrm{be}}] \tag{23}$$

Meanwhile, assuming that the voltage regulation of the filter capacitor C_{rect} is ideal and the voltage across the load remains constant, the energy transformed by the circuit during half a vibration cycle can also be expressed as:

$$W = Pt = \frac{V_{\mathrm{DC}}^2}{R_{\mathrm{L}}} \frac{T}{2} \tag{24}$$

The voltage V_{DC} across the load can be calculated by analyzing equation (23) (24).

$$V_{\mathrm{DC}} = \frac{2\omega R_{\mathrm{L}} C_{\mathrm{P}} [V_{\mathrm{OC}} + 2(\gamma - 1)V_{\mathrm{D}} - (\gamma + 1)V_{\mathrm{be}}]}{\pi + (1 - \gamma)\omega R_{\mathrm{L}} C_{\mathrm{P}}} \tag{25}$$

The output power of the system is then determined using equation (25).

$$P = \frac{V_{\mathrm{DC}}^2}{R_{\mathrm{L}}} \tag{26}$$

As demonstrated by Equation (25) and (26), the output performance of the system is intricately linked to the components utilized in the interface circuit. Thus, a well-planned design of the circuit structure can enhance the energy harvesting efficiency.

To validate the aforementioned analysis of the ESP-PSSHI circuit, we conducted simulations using the Simulink module in MATLAB. Figure 12 depicts the simulated output voltage and current waveforms for PZT.

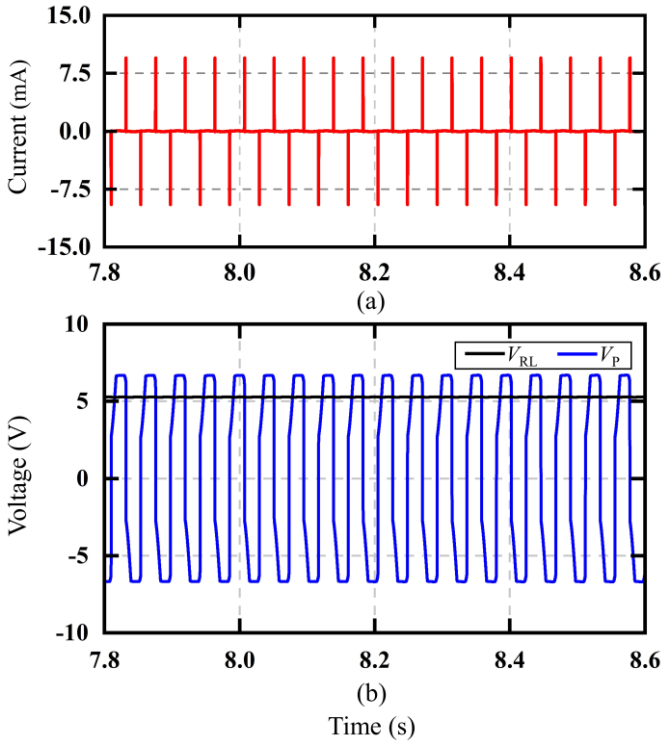

Figure 12 Theoretical waveforms of the ESP-PSSHI circuit: (a) Output current (b) Output voltage and load voltage

Figure 12 shows that the rectifier bridge turns on and the energy extraction process starts when PZT voltage reaches the conduction threshold of the rectifier bridge. Subsequently, the charge accumulated by the PZT internal capacitor is continuously transmitted to the filter capacitor and the load side. At this time, the filter capacitor's charging and discharging rates have reached dynamic equilibrium, and its voltage is nearly constant. Due to the clamping effect of the filter capacitor, the PZT voltage remains constant at this stage. When the voltage across the PZT begins to decrease, the circuit entered the disconnected state. As the voltage across the PZT decreases to a certain value, the peak detection switch turns on and the circuit enters the voltage inversion stage. The rectifier bridge is disconnected due to the low voltage after the inversion. However, the internal capacitor continues to charge as the equivalent current source operates. This charging process results in an increase in voltage across the PZT, which eventually reaches the turn-on voltage threshold of the rectifier bridge.

To assess the performance of the ESP-PSSHI circuit during operation, a comparison was made between the changes in the output waveforms of the PZT when connected to the SP-SSHI circuit and the ESP-SSHI circuit, as illustrated in Figure 13. From the figure, it can be seen that the output voltage of the PZT when it is connected to the ESP-PSSHI circuit is significantly higher than that when it is connected to the SP-PSSHI circuit, and therefore its output power will be higher. When the PZT moves to the displacement pole, the voltage at its ends does not reverse immediately due to the

presence of the switching delay, as can be seen in the Figure 13, the ESP-PSSHI circuit is able to reach the voltage inversion stage faster, thus reducing the energy loss. When the voltage inversion stage is over, the effect of the parasitic capacitance within the transistor causes the inductor L to form a resonant circuit with the internal capacitance C_P of the PZT, which reduces the voltage of the PZT after reversal. The effect of the "second inversion" is reduced by setting two inductors in the ESP-PSSHI circuit. By comparing the output voltage waveforms of the two circuits, it can be obtained that the ESP-PSSHI circuit is able to get the charge extraction stage faster after ending the voltage inversion stage, which increases the time of energy extraction and improves the energy harvesting efficiency.

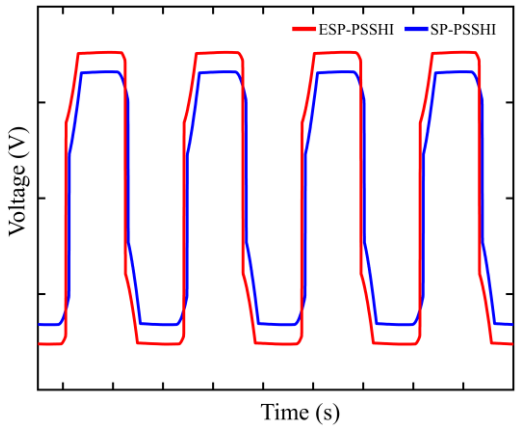

Figure 13 Comparison of P-SSHI and ESP-PSSHI output voltage

Through the above theoretical analysis and simulation, it is verified that the ESP-PSSHI circuit has better operating performance than the SP-PSSHI circuit. However, due to the impedance characteristics of the ESP-PSSHI circuit itself, the output voltage varies under different loads and operating conditions, which hinders its further application. The current operating voltage of most sensors is generally around 3.3 V, while the output voltage of the ESP-PSSHI interface circuit is generally between a few volts and tens of volts, so it is necessary to continue to optimize the ESP-PSSHI circuit so that it can transmit stable power to the sensors. Since the output voltage of the ESP-PSSHI circuit is high, we designed an optimized ESP-PSSHI circuit by combining a buck DC-DC converter with the ESP-PSSHI circuit to achieve a stable voltage output.

The design of DC-DC converter circuits using discrete components has problems such as high internal circuit losses and unstable operation. Therefore, a commercial DC-DC converter, LTC3588-1, with an integrated rectifier bridge inside and the ability to set the output voltage according to the load demand, is used in the research process and can be effectively combined with the ESP-PSSHI circuit. The optimized circuit is shown in Figure 14.

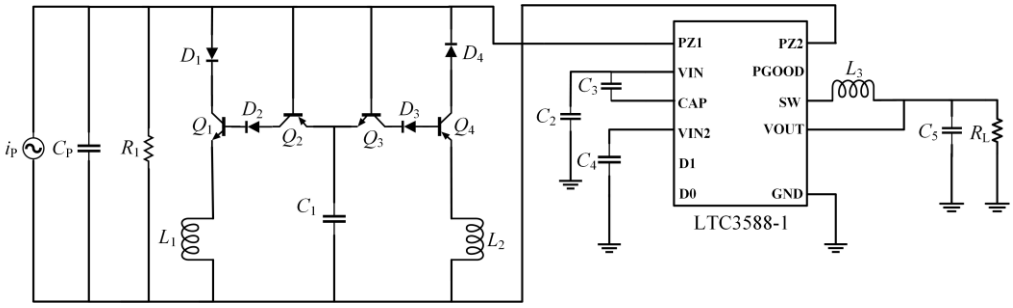

Figure 14 Schematic of the optimized ESP-PSSHI circuit

In this circuit we use a DC-DC converter instead of the rectifier bridge and filter capacitor part of the ESP-PSSHI circuit, combining the advantages of the ESP-PSSHI circuit and the DC-DC converter circuit to achieve a stable voltage output. The output performance of this optimized circuit will be verified and compared in the experiments.

4 Experiment

To prove the performance of the circuit, we built the experimental system shown in Figure 15.

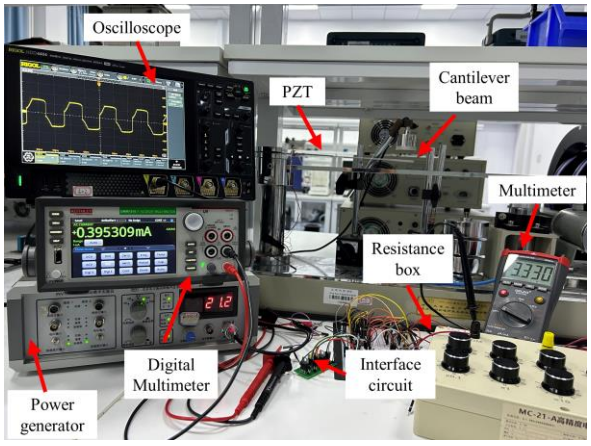

Figure 15 Experimental setup

In experiments, the electromagnet shaker is powered by the power generator (INV-1601C). The PZTs in cantilever beam biomorph are connected in series to give a higher output voltage. the PZTs current and voltage are measured by the digital multimeter (DMM7510) and the oscilloscope (RIGIO HDD4404), respectively. Then the PZTs are connected to the ESP-PSSHI interface circuit. The load voltage on the resistance box (MC-21-A) is measured by the multimeter (DEM 23+). The PEH works in a resonant state from 21.1 Hz to 21.4 Hz. The primary parameters of the entire system are shown in Table 2.

Table 2 System parameters

Devices	Parameters
Cantilever beam	300 mm×50 mm×1.5 mm
PZT	50 mm×50 mm×0.6 mm
C_P	100 nF
C_1	2.2 nF
C_{rect}	10 μF
L	22 mH

In the experiment, the resistance box was used to change the load value. The output voltages of the SEH, SP-PSSHI and ESP-PSSHI were recorded, and the output power of each circuit were calculated.

To investigate the output performance of the ESP-PSSHI circuit under different excitation levels, the PEH is adjusted to work at the resonance frequency, three different excitation levels of V_{PP} (PZT output voltage peak-to-peak value) equal to 12 V, 18 V and 24 V were taken to explore the output performance of the interface circuit. The output power curves of the SEH circuit, SP-PSSHI circuit and ESP-PSSHI circuit with respect to the load are shown in Figure 16. From the overall experimental results, the output power of the ESP-PSSHI circuit is significantly higher than that of the SEH circuit and the SP-PSSHI circuit at different V_{PP}. It can be observed from Figure 16 (c), the output power of the ESP-PSSHI circuit reaches up to 518 μW under three different excitations. The output power of the ESP-PSSHI circuit has the largest improvement compared to the SEH circuit at a V_{PP} of 12V, and the output power of the ESP-PSSHI circuit has the largest improvement compared to the SP-PSSHI circuit at a V_{PP} of 24 V.

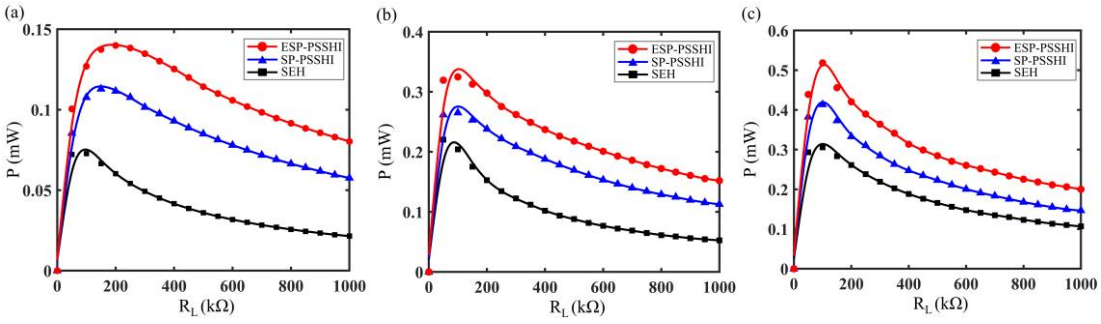

Figure 16 Circuit output power versus load at different excitation levels: (a) V_{pp}=12 V; (b) V_{pp}=18 V; (c) V_{pp}=24 V

Subsequently, the output performance of the three circuits was tested with the same load at different frequencies. In the experiments, three different loads of 100 kΩ, 150 kΩ and 200 kΩ were selected. The output power of the three circuits at the excitation frequency of 20.5Hz-22.5Hz is shown in Figure 17. From the overall experimental

results, the output power of the interface circuit is the maximum at the resonance frequency, and decreases continuously as the frequency increases or decreases. As the load increases, the output power of each circuit is also increasing, and when the load is 200 kΩ, the output power of the ESP-PSSHI circuit improves the most compared to the other two circuits, and at this time, the output power of the ESP-PSSHI circuit is 2.42 times as much as that of the SEH circuit and 1.16 times as much as that of the SP-PSSHI circuit. It can be observed in the experiment that the change of load does not have a great influence on the resonance frequency of the system. This is because the PEH used in this study works under weak electromechanical coupling conditions, the change of electro-induced damping has little effect on the resonance frequency of the system.

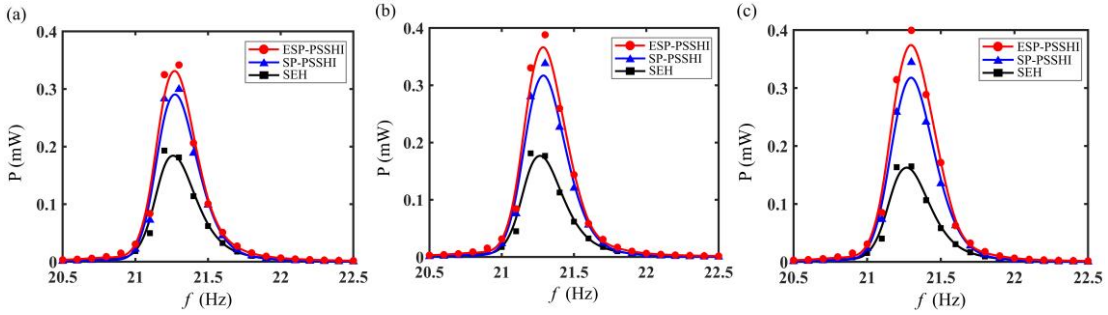

Figure 17 Relationship between circuit output power and excitation frequency at different loads: (a) R_L=100 kΩ; (b) R_L=150 kΩ; (c) R_L=200 kΩ

Through experiments, we tested the time for the capacitor to reach steady state when the PZT charges the different capacitor through the LTC3588 module and the optimized ESP-PSSHI circuit, respectively. An oscilloscope was used to record the output voltage as shown in Figure 18, with the output voltage set to a regulated output of 3.3 V. Experiments show that the optimized ESP-PSSHI circuit has a significantly higher charging rate than the LTC3588-1 circuit at different capacitances. The optimized ESP-PSSH circuit reduces the time for the energy storage element to reach the steady-state voltage, and based on the relationship between power and capacitor charging time, the output power of the optimized ESP-PSSHI circuit is 1.5 times the output power of the LTC3588-1 circuit.

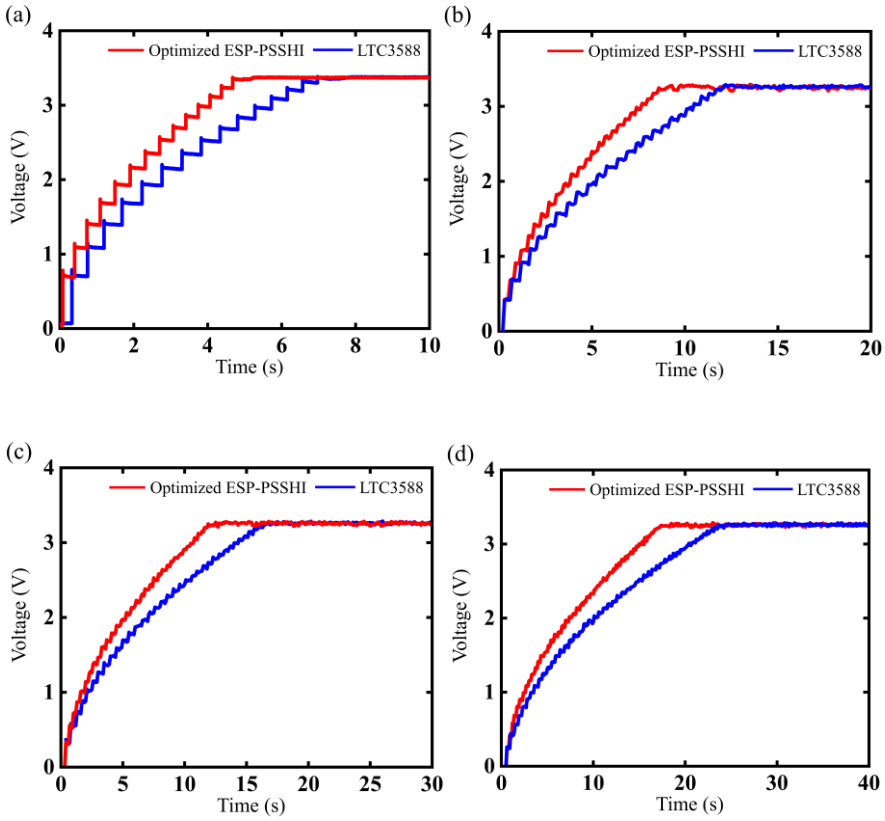

Figure 18 Charging experiment with different capacitors: (a) 100 μF (b) 220 μF (c) 330 μF (d) 470 μF

Figure 19 shows the experimental and theory results of the ESP-PSSHI circuit output power variation with the load. From the figure, it can be seen that the maximum output power of the experiment is less than the maximum output power of the simulation, but the observed shift in trend is in accordance with the calculated findings. The reason leading to this phenomenon is the existence of various forms of energy loss in the circuit. These losses mainly include thermal energy losses caused by the internal resistance of the rectifier diode and other resistive components and power transmission losses on the inductor. In addition, a simplified equivalent circuit is applied in the simulation process without considering the backward coupling of the circuit, which results in a higher energy output in the simulation than the experimental output [45].

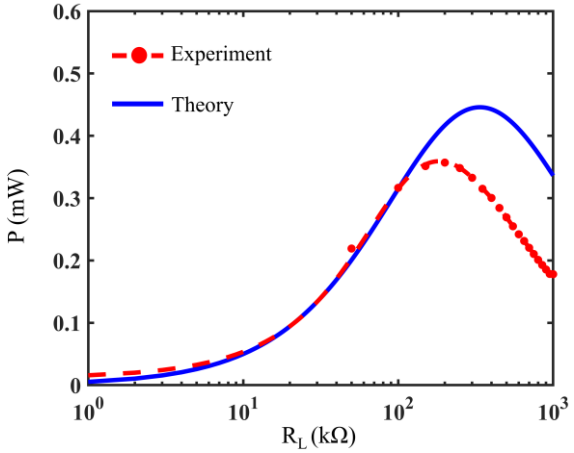

Figure 19 Output power of the ESP-PSSHI circuit

5 Conclusion

In this paper, we first propose a highly efficient self-powered PZT energy harvesting interface circuit. By optimizing the peak detection switch, the switching delay is reduced, and the energy loss resulting from the "second inversion" in the circuit is mitigated, thereby enhancing the efficiency of energy extraction. The feasibility of the circuit is verified by simulation and experiment. The experimental results show that the ESP-PSSHI circuit exhibits higher output power than the SP-PSSHI circuit and the SEH circuit at different excitation levels. When the PZT output voltage peak-to-peak value is 24 V, the maximum output power of the ESP-PSSHI circuit can reach 518 μW. In this case, the output power is 1.24 times and 1.67 times that of the SP-PSSHI circuit and the SEH circuit, respectively. At the same load and different frequencies, the ESP-PSSHI circuit also shows higher output power than the SP-PSSHI circuit and the SEH circuit. When the load is 200 kΩ, the maximum output power of the ESP-PSSHI circuit is 1.16 times and 2.42 times that of the SP-PSSHI circuit and the SEH circuit, respectively. In order to make the circuit achieve impedance matching, we optimized the ESP-PSSHI circuit by adding a DC-DC converter to the ESP-PSSHI circuit, and finally achieved a stable power output. The average output power of the optimized ESP-PSSHI circuit is 133 μW, which is 1.4 times that of the LTC3588-1 circuit. This circuit can realize energy harvesting without external device power and control, meet the needs of the current wireless sensor network nodes to achieve self-powered. Furthermore, it provides a new method for implementing SSHI circuits in practice and also provides new ideas for the use of nonlinear circuits in combination with DC-DC modules. The highlights of this paper are shown below:

(1) An efficient self-powered parallel SSHI (ESP-PSSHI) interface circuit is proposed.

(2) The ESP-PSSHI circuit enhances the passive peak detection switch, simplifies the circuit topology, reduces switching delay and minimizes the “second inversion”.

(3) The optimized design by combining the advantages of the ESP-PSSHI circuit and the DC-DC converter circuit achieves a stable voltage output.

(4) Both the simulation and experimental results demonstrate the enhanced vibration energy harvesting capability of the developed circuit.

Although the proposed circuit has better output power performance than the SEH circuit and the SP-PSSHI circuit, it can be observed from the experiment that when the PEH deviates from the resonant frequency range, the output power of the ESP-PSSHI circuit decreases a lot. In the future work, the circuit structure should be further improved around the broadband to adapt to the complex and changeable external vibration environment. At the same time, the PEH used in this study works under weak electromechanical coupling conditions, and the influence of electromechanical coupling coefficient on energy harvester and interface circuit is not fully considered. In addition, there is still room for improvement in the combined design of nonlinear circuits and DC-DC modules to further improve energy conversion efficiency.

Acknowledgement.

This project is supported by the National Key R&D Program of China (Grant No. 2022YFB2603200), the Program of National Natural Science Foundation of China (Grant Nos. 51805298, 12072267), Natural Science Foundation of Shandong Province (ZR2019PEE015), Young Scholars Program of Shandong University, Weihai (Grant No. 20820201004) and Fundamental Research Funds for the Central Universities (Grant No. 2019ZRJC006).

References

[1] Sawane M, Prasad M. MEMS piezoelectric sensor for self-powered devices: A review. Materials Science in Semiconductor Processing. 2023;158:107324.
[2] Gu S, Xu W, Xi K, Luo A, Fan K, Wang F. High-performance piezoelectric energy harvesting system with anti-interference capability for smart grid monitoring. Renewable Energy. 2024;221:119742.
[3] Yu Y, Zhao X, Ge H, Ye L. A self-powered piezoelectric Poly(vinyl alcohol)/Polyvinylidene fluoride fiber membrane with alternating multilayer porous structure for energy harvesting and wearable sensors. Composites Science and Technology. 2024;247:110429.
[4] Demouron Q, Morel A, Gibus D, Benhemou A, Badel A. A comparative analysis of parallel SSHI and SEH for bistable vibration energy harvesters. Smart Materials and Structures. 2023;32(12).
[5] Younas O, Li P, Wen Y. A compact self-powered inductor-less piezoelectric energy harvesting circuit using gyrator. Smart Materials and Structures. 2024;33(6).

[6] Zhang B, Li H, Zhou S, Liang J, Gao J, Yurchenko D. Modeling and analysis of a three-degree-of-freedom piezoelectric vibration energy harvester for broadening bandwidth. Mechanical Systems and Signal Processing. 2022;176:109169.
[7] Zhang B, Zhou H, Zhao X, Gao J, Zhou S. Design and experimental analysis of a piezoelectric energy harvester based on stacked piezoceramic for nonharmonic excitations. Energy. 2023;282:128948.
[8] Li Z, Wang J, Law MK, Du S, Liang J, Cheng X, et al. Piezoelectric Energy Harvesting Interface Using Self-Bias-Flip Rectifier and Switched-PEH DC–DC for MPPT. IEEE Journal of Solid-State Circuits. 2023:1-12.
[9] Chen K, Zhuo J, Liu W, Huang Y, Hua C, Zhu Q, et al. Self-sensed, self-adapted and self-powered piezoelectric generator architecture by synchronous circuits of autonomous parameter tuning. Energy Conversion and Management. 2024;300:117919.
[10] Cao X, Chiang WJ, King YC, Lee YK. Electromagnetic Energy Harvesting Circuit With Feedforward and Feedback DC–DC PWM Boost Converter for Vibration Power Generator System. IEEE Transactions on Power Electronics. 2007;22(2):679-85.
[11] Dell'Anna F, Dong T, Li P, Wen Y, Yang Z, Casu MR, et al. State-of-the-Art Power Management Circuits for Piezoelectric Energy Harvesters. IEEE Circuits and Systems Magazine. 2018;18(3):27-48.
[12] Brenes A, Morel A, Juillard J, Lefeuvre E, Badel A. Maximum power point of piezoelectric energy harvesters: a review of optimality condition for electrical tuning. Smart Materials and Structures. 2020;29(3):033001.
[13] Xu Y, Xian T, Chen C, Wang G, Wang M, Shi W. Mathematical modeling and parameter optimization of a stacked piezoelectric energy harvester based on water pressure pulsation. Energy. 2024;292:130530.
[14] Zhang B, Liu H, Zhou S, Gao J. A review of nonlinear piezoelectric energy harvesting interface circuits in discrete components. Applied Mathematics and Mechanics. 2022;43(7):1001-26.
[15] Hu B, Li Z, Liu H, Zhang B, Zhou S. A Self-Powered Rectifier-Less Series-Synchronized Switch Harvesting on Inductor (S-SSHI) Interface Circuit for Flutter-Based Piezoelectric Energy Harvesters. IEEE Instrumentation & Measurement Magazine. 2023;26(3):5-13.
[16] Ottman GK, Hofmann HF, Lesieutre GA. Optimized piezoelectric energy harvesting circuit using step-down converter in discontinuous conduction mode. IEEE Transactions on Power Electronics. 2003;18(2):696-703.
[17] Guyomar D, Badel A, Lefeuvre E, Richard C. Toward energy harvesting using active materials and conversion improvement by nonlinear processing. IEEE Transactions on Ultrasonics, Ferroelectrics, and Frequency Control. 2005;52(4):584-95.
[18] Taylor GW, Burns JR, Kammann SA, Powers WB, Welsh TR. The Energy Harvesting Eel: a small subsurface ocean/river power generator. IEEE Journal of Oceanic Engineering. 2001;26(4):539-47.
[19] Lefeuvre E, Badel A, Richard C, Guyomar D. Piezoelectric Energy Harvesting Device Optimization by Synchronous Electric Charge Extraction. Journal of Intelligent Material Systems and Structures. 2005;16(10):865-76.
[20] Wu Y, Badel A, Formosa F, Liu W, Agbossou AE. Piezoelectric vibration energy harvesting by optimized synchronous electric charge extraction. Journal of Intelligent Material Systems and Structures. 2012;24(12):1445-58.
[21] Brenes A, Morel A, Gibus D, Yoo CS, Gasnier P, Lefeuvre E, et al. Large-bandwidth piezoelectric energy harvesting with frequency-tuning synchronized electric charge extraction. Sensors and Actuators A: Physical. 2020;302:111759.
[22] Chen Z, Xia Y, Shi G, Wang X, Xia H, Ye Y. Self-Powered Multi-Input Serial SSHI Interface Circuit With Arbitrary Phase Difference for Piezoelectric Energy Harvesting. IEEE Transactions on Power Electronics. 2021;36(8):9183-92.
[23] Wang X, Xia Y, Shi G, Xia H, Chen Z, Ye Y, et al. A Self-Powered Rectifier-Less Synchronized Switch Harvesting on Inductor Interface Circuit for Piezoelectric Energy Harvesting. IEEE Transactions on Power Electronics. 2021;36(8):9149-59.

[24] Sanchez DA, Leicht J, Hagedorn F, Jodka E, Fazel E, Manoli Y. A Parallel-SSHI Rectifier for Piezoelectric Energy Harvesting of Periodic and Shock Excitations. IEEE Journal of Solid-State Circuits. 2016;51(12):2867-79.
[25] Zhang Z, Xiang H, Tang L. Modeling, analysis and comparison of four charging interface circuits for piezoelectric energy harvesting. Mechanical Systems and Signal Processing. 2021;152:107476.
[26] Lu S, Boussaid F. A Highly Efficient P-SSHI Rectifier for Piezoelectric Energy Harvesting. IEEE Transactions on Power Electronics. 2015;30(10):5364-9.
[27] Lallart M, Wu W-J, Hsieh Y, Yan L. Synchronous inversion and charge extraction (SICE): a hybrid switching interface for efficient vibrational energy harvesting. Smart Materials and Structures. 2017;26(11):115012.
[28] Liang J, Zhao Y, Zhao K. Synchronized Triple Bias-Flip Interface Circuit for Piezoelectric Energy Harvesting Enhancement. IEEE Transactions on Power Electronics. 2019;34(1):275-86.
[29] Du S, Amaratunga GAJ, Seshia AA. A Cold-Startup SSHI Rectifier for Piezoelectric Energy Harvesters With Increased Open-Circuit Voltage. IEEE Transactions on Power Electronics. 2019;34(1):263-74.
[30] Badr AO, Lou E, Tsui YY, Moussa WA. A High Efficiency AC/DC NVC-PSSHI Electrical Interface for Vibration-Based Energy Harvesters. IEEE Transactions on Circuits and Systems I: Regular Papers. 2020;67(1):346-55.
[31] Lallart M, Guyomar D. An optimized self-powered switching circuit for non-linear energy harvesting with low voltage output. Smart Materials and Structures. 2008;17(3):035030.
[32] Liang J, Liao WH. Improved Design and Analysis of Self-Powered Synchronized Switch Interface Circuit for Piezoelectric Energy Harvesting Systems. IEEE Transactions on Industrial Electronics. 2012;59(4):1950-60.
[33] Zhang B, Liu H, Hu B, Zhou S. Analysis and optimization of self-powered parallel synchronized switch harvesting on inductor circuit for piezoelectric energy harvesting. Smart Materials and Structures. 2022;31(9):095040.
[34] Kong N, Ha DS, Erturk A, Inman DJ. Resistive Impedance Matching Circuit for Piezoelectric Energy Harvesting. Journal of Intelligent Material Systems and Structures. 2010;21(13):1293-302.
[35] Chen N, Wei T, Ha DS, Jung HJ, Lee S. Alternating Resistive Impedance Matching for an Impact-Type Microwind Piezoelectric Energy Harvester. IEEE Transactions on Industrial Electronics. 2018;65(9):7374-82.
[36] Wang Q, Li S, Oh JAS, Wu T. Electrical impedance matching based on piezoelectric ceramics for energy harvesting application. Materials Technology. 2020;35(9-10):650-5.
[37] Li S, Roy A, Calhoun BH. A Piezoelectric Energy-Harvesting System With Parallel-SSHI Rectifier and Integrated Maximum-Power-Point Tracking. IEEE Solid-State Circuits Letters. 2019;2(12):301-4.
[38] Chew ZJ, Zhu M. Adaptive Maximum Power Point Finding Using Direct VOC/2 Tracking Method With Microwatt Power Consumption for Energy Harvesting. IEEE Transactions on Power Electronics. 2018;33(9):8164-73.
[39] Sharma Y, Liu M, Jung H, Zuo L. Adaptive damping tuning and circuit implementation for broad bandwidth energy harvesting. Smart Materials and Structures. 2020;29(11):115049.
[40] Lan C, Liao Y, Hu G. A unified equivalent circuit and impedance analysis method for galloping piezoelectric energy harvesters. Mechanical Systems and Signal Processing. 2022;165:108339.
[41] Shim M, Kim J, Jeong J, Park S, Kim C. Self-Powered 30 μW to 10 mW Piezoelectric Energy Harvesting System With 9.09 ms/V Maximum Power Point Tracking Time. IEEE Journal of Solid-State Circuits. 2015;50(10):2367-79.
[42] Garbuio L, Lallart M, Guyomar D, Richard C, Audigier D. Mechanical Energy Harvester With Ultralow Threshold Rectification Based on SSHI Nonlinear Technique. IEEE Transactions on Industrial Electronics. 2009;56(4):1048-56.
[43] Hong J, Chen F, He M, Wang S, Chen W, Guan M. Study of a low-power-consumption piezoelectric energy harvesting circuit based on synchronized

switching technology. Energies. 2019;12(16):3166.
[44] Lefeuvre E, Badel A, Richard C, Petit L, Guyomar D. A comparison between several vibration-powered piezoelectric generators for standalone systems. Sensors and Actuators A: Physical. 2006;126(2):405-16.
[45] Yang Y, Tang L. Equivalent Circuit Modeling of Piezoelectric Energy Harvesters. Journal of Intelligent Material Systems and Structures. 2009;20(18):2223-35.